Thermal spin molecular logic gates modulated by an electric field

Xingyi Tan(谭兴毅)[1,†], Qiang Li(李强)[2], and Dahua Ren(任达华)[2]

[1] *Department of Physics, Chongqing Three Gorges University, Wanzhou* 404100, *China*
[2] *College of Intelligent Systems Science and Engineering, Hubei Minzu University, Enshi* 445000, *China*

(Received 2 June 2022; revised manuscript received 2 August 2022; accepted manuscript online 16 August 2022)

Logic gates are fundamental structural components in all modern digital electronic devices. Here, nonequilibrium Green's functions are incorporated with the density functional theory to verify the thermal spin transport features of the single-molecule spintronic devices constructed by a single molecule in series or parallel connected with graphene nanoribbons electrodes. Our calculations demonstrate that the electric field can manipulate the spin-polarized current. Then, a complete set of thermal spin molecular logic gates are proposed, including AND, OR, and NOT gates. The mentioned logic gates enable different designs of complex thermal spin molecular logic functions and facilitate the electric field control of thermal spin molecular devices.

Keywords: thermal spin molecular logic gates, electric field, single-molecule

PACS: 71.15.Mb, 61.72.uj, 74.78.Fk **DOI:** 10.1088/1674-1056/ac89e5

1. Introduction

Based on Moore's law, the number of transistors on a microchip doubles any two years.[1] The mentioned exponential growth speed leads to two problems. Firstly, the miniaturization of traditional silicon-based electronic devices will quickly attain their corresponding maximum efficiency.[2] Secondly, the continuous miniaturization of physical devices increase the waste heat significantly. Molecular electronics can be utilized to solve the first problem. Particularly, in 1993, de Silva *et al.*[3] employed fluorescent signaling to construct the first molecular AND gate, initiating the area of molecular logic gates (MLGs). After that, several strategies have been adopted to construct MLGs.[4] On the other hand, spintronics devices are also utilized to solve the first problem. Some spin logic devices and many bionic or mimicry properties based on spintronics have been demonstrated.[5–9] Recently, spin and molecular electronics have been combined to develop molecular spintronic electronics as a spin-polarized type of molecular electronics.[10,11] Molecular spintronic devices have significant applications in next-generation electronics, particularly over traditional spintronics devices, such as biocompatibility, plasticity, etc.[12]

On the other hand, spin caloritronics, taking advantage of spintronics and thermoelectronics, provide a good solution for the second problem because the spin currents and voltages of a spin caloritronic device are generated only via a temperature gradient without employing an electrical bias.[13–18] In experiment, Sierra *et al.* have detected the thermoelectric spin voltage due to the thermally driven spin-polarized currents in the FM graphene nanoribbons.[19] In theory, Zhao *et al.* employed planar four-coordinate Fe complexes-based molecular,[20] Mn-porphyrin trimer molecular,[21] Mn phthalocyanine molecular,[22,23] and a hybrid molecular junction comprising a planar four-coordinate Fe molecule and a 15,16-dinitrile dihydropyrene/cyclophanediene molecule[24,25] to construct thermal spin molecular Boolean logic gates like AND, NOT, XOR, and OR. All these thermal spin molecular Boolean logic gates contain metal atoms, providing the magnetic source of the devices. Nevertheless, applying external magnetic fields in various directions on metal atoms within a narrow area is challenging.[25] On the contrary, owing to the rapid development of scanning probe technology, electric field regulation technology is relatively mature. Therefore, it is meaningful and necessary to find new thermal spin molecular Boolean logic gates, which are controlled only by the electric field.

In this paper, some single-molecule spintronic devices were constructed by a single molecule in series or parallel connected with graphene nanoribbons electrodes and the thermal spin transport features of these devices were investigated. Our calculations demonstrated that the electric field can control the spin-polarized currents. Then, three thermal spin molecular logic gates were proposed, including AND, OR, and NOT gates. The mentioned logic gates enable different designs of complex thermal spin molecular logic functions and facilitate the electric field control of thermal spin molecular devices.

2. Computation method

Spin density functional theory (DFT) was combined with the nonequilibrium Green's function (NEGF) technique in the Atomistix ToolKit package[26,27] to carry out the geometrical optimization and electronic structure computations. The exchange–correlation potential was derived from the double

[†]Corresponding author. E-mail: tanxy@sanxiau.edu.cn

© 2023 Chinese Physical Society and IOP Publishing Ltd

numerical plus polarization (DNP) basis set and the generalized gradient approximation (GGA)[28,29] technique. In order to facilitate the convergence of the optimization algorithm, the atoms' spatial positions were relaxed, while the maximum force tolerance was selected as 0.01 eV/Å. The energy convergence standard and the cut-off energy were chosen as 1×10^{-5} eV and 150 Hartree, respectively. To obtain the thermal spin-related transport currents, similar core electrons, exchange–correlation potentials, and cut-off energy were chosen. Moreover, a $1\times1\times100$ Monkhorst–Pack k-point grid was adopted to achieve precise results.

Based on the Landauer–Büttiker formalism, the devices' spin-related currents can be calculated through the relation[30]

$$I^{\uparrow(\downarrow)}=\frac{e}{h}\int_{-\infty}^{\infty}\left\{T^{\uparrow(\downarrow)}(E)\left[f_{\mathrm{L}}(E,T_{\mathrm{L}})-f_{\mathrm{R}}(E,T_{\mathrm{R}})\right]\right\}\mathrm{d}E, \quad (1)$$

where e describes the electron charge, h stands for the Planck constant, $T_{\mathrm{L(R)}}$ describes the left (right) electrode temperature, and $f_{\mathrm{L(R)}}(E,T_{\mathrm{L(R)}})$ describes the left (right) electrode's average Fermi–Dirac distribution, as described by

$$f_{\mathrm{L(R)}}\left(E,T_{\mathrm{L(R)}}\right)=\left\{1+\exp\left[E-\mu_{\mathrm{L(R)}}/k_{\mathrm{B}}T_{\mathrm{L(R)}}\right]\right\}^{-1}, \quad (2)$$

where $\mu_{\mathrm{L(R)}}$ and $T_{\mathrm{L(R)}}$ stand for the left (right) electrode's chemical potential and temperature, respectively. k_{B} describes the Boltzmann constant, and $T^{\uparrow(\downarrow)}(E)$ represents the spin-related transport parameter, represented by

$$T^{\uparrow(\downarrow)}(E)=\mathrm{Tr}[\Gamma_{\mathrm{L}}G^{\mathrm{r}}\Gamma_{\mathrm{R}}G^{\mathrm{a}}], \quad (3)$$

where $G^{\mathrm{r(a)}}$ stands for the central region's retarded (advanced) Green's function, while $\Gamma_{\mathrm{L(R)}}$ describes the interaction between the central dispersion region and the left (right) contact.

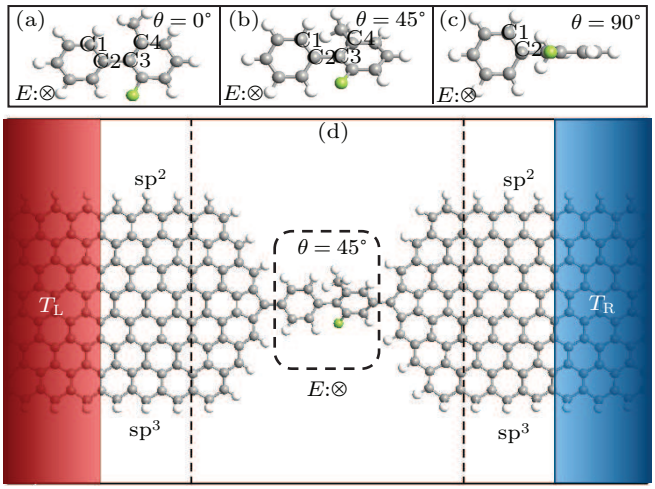


Fig. 1. (a)–(c) The atomic structure of the molecule studied in this work. The C1, C2, C3, and C4 stand for the atoms describing the torsion angle. (d) The schematic illustration of the thermal spin device ($\theta=45°$ as an example).

Two connected benzene rings were taken with a methyl group on one of them, while a fluorine atom was attached to them to generate a dipole moment on them to create the torsion angle variation under the electric field, as presented in Figs. 1(a)–1(c). This way has also been utilized by Vergniory *et al.*[31] This molecule is covalently bridged between two 8-ZGNNR electrodes, where there are 8 zigzag carbon chains along its width with asymmetric edge hydrogenations, with an edge passivated by a single H atom (sp^2), while two H atoms (sp^3) passivate the other one. In our system, the left electrode temperature (T_{L}) is greater than that of the right one (T_{R}). The mentioned temperature difference, namely, $\Delta T=T_{\mathrm{L}}-T_{\mathrm{R}}$, generates the thermal spin-related currents.

3. Results and discussion

3.1. The molecule's ground state

To analyze the benzene ring-ring rotation, the atomic coordinates are optimized while stabilizing the torsion angle of θ (C1–C2 –C3–C4), as presented in Figs. 1(a) and 1(b). The direction of the electric field is straight into the page, as shown in Fig. 1. The ground state total energy is calculated with respect to the torsion angle and exerted electric field, as presented in Fig. 2. As shown in Fig. 2, the $\theta=0°$ planar conformation differs from the ground state under zero electric field, which is at 45°. This is reasonable since there is a dipole moment at one ring. Furthermore, at $E=0.2$ V/Å, the molecule has the largest energy. This is understandable because the $-CH_3$ steric effects are dominant at small torsion angle (θ) and electric field.[31,32] Interestingly, when the electric field $E\geq0.4$ V/Å, the most stable state is the $\theta=90°$ one. Therefore, this state could be easily obtained experimentally.

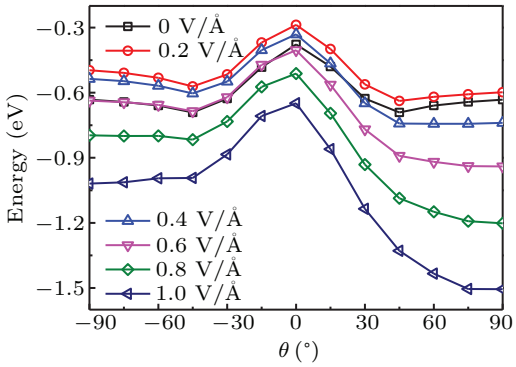


Fig. 2. The whole energy versus the torsion angle (θ) for different applied electric fields.

3.2. Thermally-driven spin transport properties

In Figs. 3(a) and 3(b), we firstly focus on the transmission spectra of $E=0$ and $E\geq0.4$ V/Å states, which are the mostly intuitive representation of the transport properties. For the convenience of the following description, $E=0$ and $E\geq0.4$ V/Å states are marked as E_0 and E_1, respectively. The E_0 and E_1 states have similar transmission spectra, that is, the conductance channel for the spin-up (SU) and spin-down (SD) transmission is open in the energy areas $[-0.54, -0.25]$ eV and $[0.25, 0.50]$ eV, respectively. An evident transmission gap

is near the Fermi level, while the 8-ZαGYNR band structure generates the mentioned transmission properties. However, the transmission coefficient of the E_0 state is much greater than that of E_1.

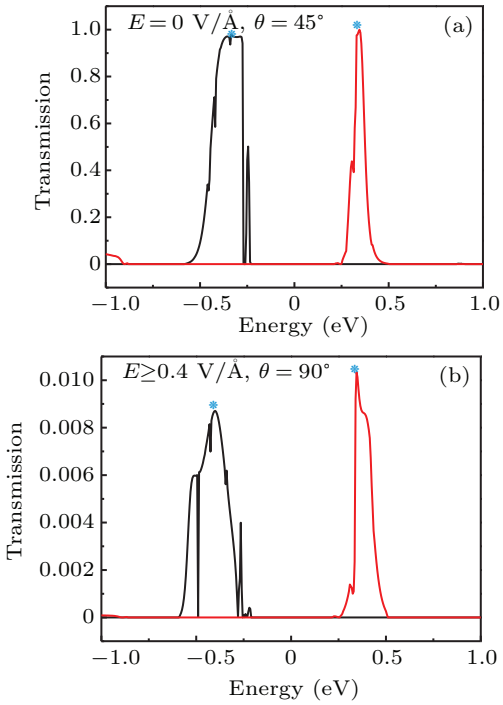


Fig. 3. The thermal spin molecular device's spin-related transmission spectra, (a) E_0, (b) E_1. Here, the red and black lines indicate the SD and SU electrons, respectively.

Therefore, when the E_0 changes to the E_1, the device is predicted to switch from the logic on-state to the off-state. To grasp this conjecture, Fig. 4 shows the spin-resolved transmission eigenstates at the most significant values of the transmission spectra (marked as blue stars in Fig. 3). To all appearances, the SU and SD electrons' transmission eigenstates are continuously distributed throughout the device for the E_0 forms, as shown in Figs. 4(a) and 4(b). At the same time, the SU and SD electrons are thoroughly localized at the left electrode and the center region and almost disappear at the right electrode region for the E_1 forms, resulting in a blockade of electron transport, as shown in Figs. 4(c) and 4(d).

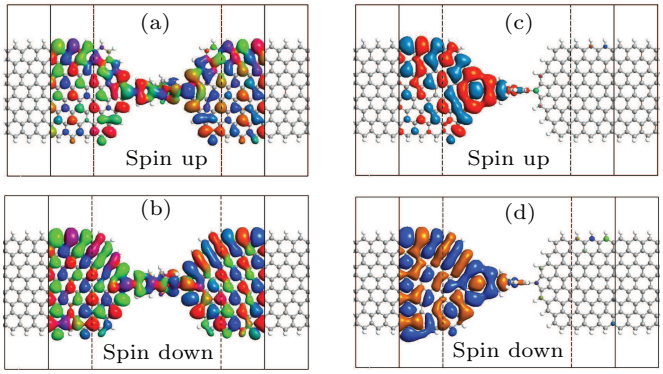


Fig. 4. Spin-resolved transmission eigenstates of the thermal spin molecular devices under zero bias, (a), (b) E_0, (c), (d) E_1. The isovalues are 0.1 Å$^{-3/2}$.

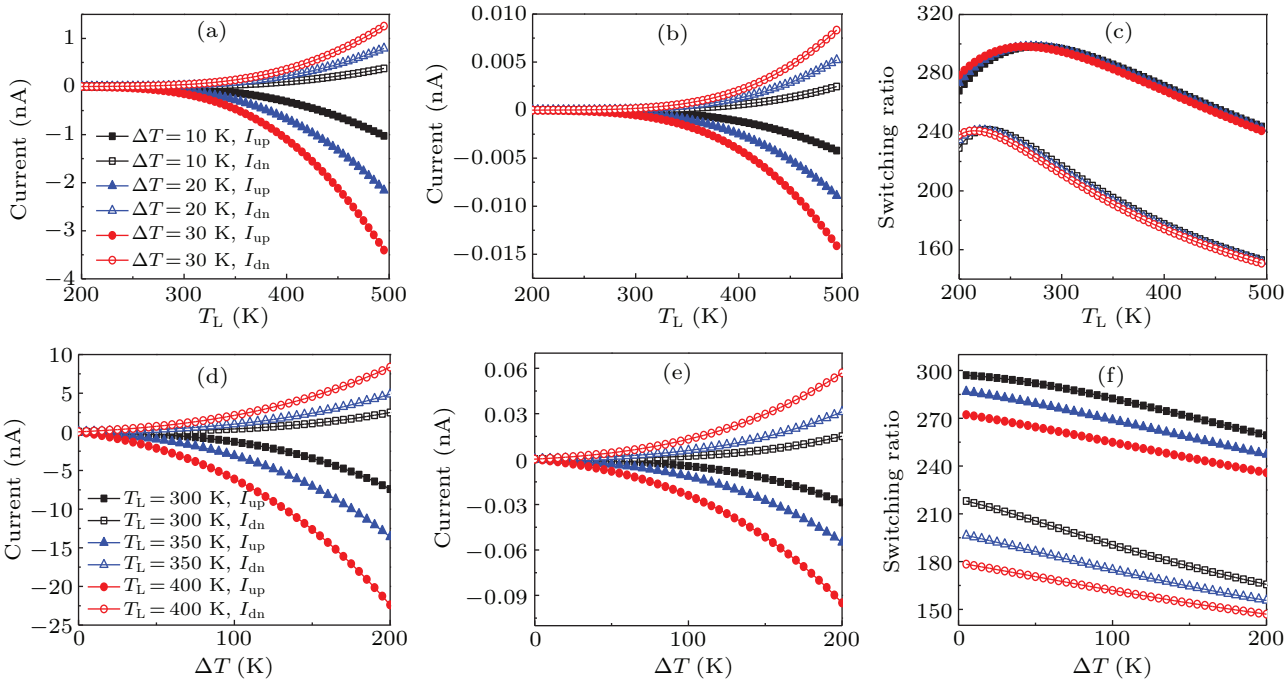


Fig. 5. The thermally driven spin-related currents I_{up} and I_{dn} in the thermal spin molecular devices with respect to T_L and ΔT, (a) and (d) E_0; (b) and (e) E_1. (c) and (f) The corresponding switching ratio of the thermal spin devices versus T_L and ΔT, respectively.

The thermal SU (I_{up}) and SD currents (I_{dn}) of the E_0 and E_1 with respect to the device temperature T_L for three temperature gradients (ΔT = 10 K, 20 K, and 30 K) are presented in Figs. 5(a) and 5(b). Firstly, one can see that E_0 and E_1 have similar transport properties, except the I_{up} and I_{dn} of E_0 are much larger than those E_1. When $T_L < 230$ K, I_{up} =0, indicating that a threshold temperature (T_{th-up}) exists and if $T_L > 230$ K, I_{up} increases with increasing the temperature T_L,

Meanwhile, I_{dn} has a different threshold temperature (T_{th-dn}) with 260 K and shows a similar transport behavior with that of I_{up}. Various threshold temperatures may be caused by various transmission areas for the E_0 and E_1 devices' spin-related transmission spectra, as presented in Fig. 3. To compare the transports of E_0 and E_1, the switching ratios ($SR = I_{up,0}/I_{up,1}$; or $SR = I_{dn,0}/I_{dn,1}$, where $I_{up/dn,0}$, $I_{up/dn,1}$ are I_{up} or I_{dn} for E_0 and E_1, respectively) are shown in Fig. 5(c). It can be seen that SR has larger values, meaning that E_0 and E_1 can design thermal spin molecular Boolean logic gates.

3.3. Thermal spin molecular gates

The AND and OR gates comprise two inputs (A and B) and a single output (Y). The E_0 and E_1 correspond to A and B, respectively, while the resistance state for I_{up} or I_{dn} corresponds to Y. Particularly, E_0 and E_1 stand for logic 1 and logic 0 for A and B, and the high and low currents I_{up} or I_{dn} stand for logic 1 and logic 0 for Y, respectively.

To obtain the AND gate, two molecules are concatenated to the graphene nanoribbons electrode. Figure 6 shows the spin-resolved transmission eigenstates at the largest values of the transmission spectra (see the support materials in Fig. 1). To all appearances, the transmission eigenstates of the SU and SD electrons are continuously distributed throughout the device for the E_0/E_0, while the transmission eigenstate of the SU and SD electrons are thoroughly localized and approximately disappear at the right electrode region for the E_0/E_1, E_1/E_0, and E_1/E_1, blockading the electron transport. These calculated results indicate that the AND logical relationship is established. To obtain the OR gate, two molecules are connected parallel to the graphene nanoribbons electrode.

Figure 7 shows the spin-resolved transmission eigenstates at the most significant values of the transmission spectra (see the support materials in Fig. 1). To all appearances, the transmission eigenstates of the SU and SD electrons are continuously distributed throughout the device for the E_0/E_0, E_1/E, and E_0/E_1 In contrast, the SU and SD electrons' transmission eigenstates are thoroughly localized and almost disappear at the right electrode region for the E_1/E_1, blockading the electron transport. These calculated results indicate that the OR logical relationship is established. The NOT gate involves a single input A and a single output Y. The E_0/E_1 corresponds to A, and the resistance state for I_{up} or I_{dn} corresponds to Y. Particularly, E_0/E_1 stands for logic 1 and logic 0 for A, while the low and high currents I_{up} or I_{dn} stand for logic 1 and logic 0 for Y, respectively. As mentioned in the transport property part, the NOT logical relationship is established. The inputs, output, truth table, and circuit symbols for thermal spin MLGs are summarized in Fig. 8 (including AND, OR, and NOT gates).

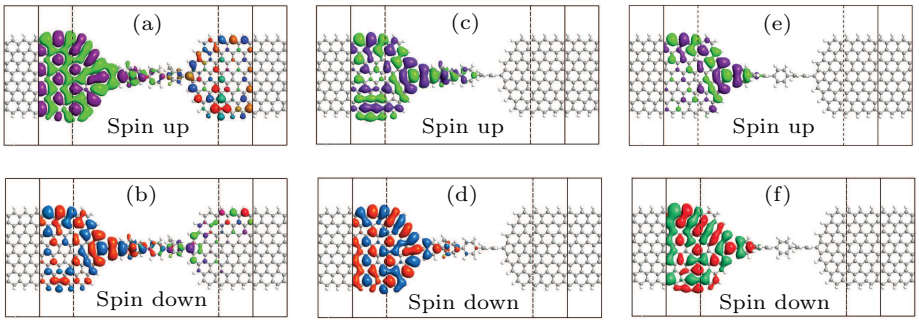


Fig. 6. Spin-resolved transmission eigenstates of the thermal spin molecular devices under zero bias for in series, (a), (b) E_0/E_0; (c), (d) E_0/E_1 or $E1_0/E_0$; (e), (f) E_1/E_1. The isovalues are 0.1 Å$^{-3/2}$.

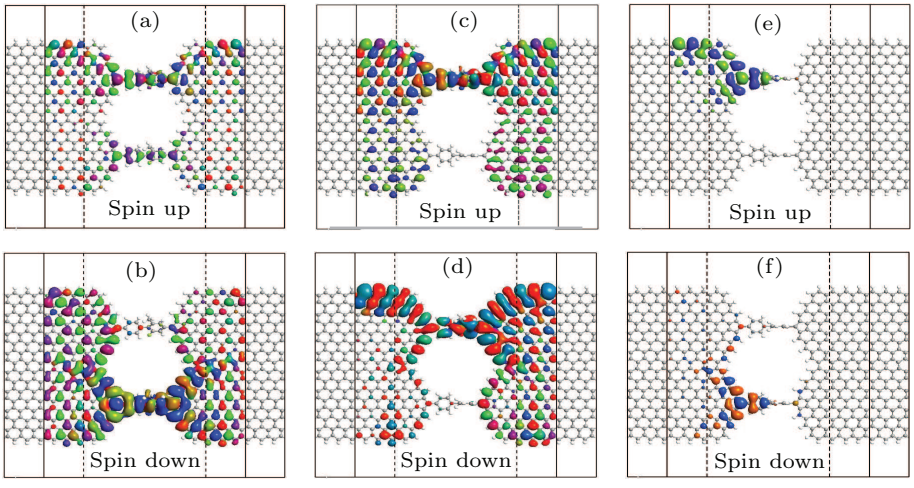


Fig. 7. Spin-resolved transmission eigenstates of the thermal spin molecular devices under zero bias for the parallel connection, (a), (b) E_0/E_0; (c), (d) E_0/E_1 or $E1_0/E_0$; (e), (f) E_1/E_1. The isovalues are 0.1 Å$^{-3/2}$.

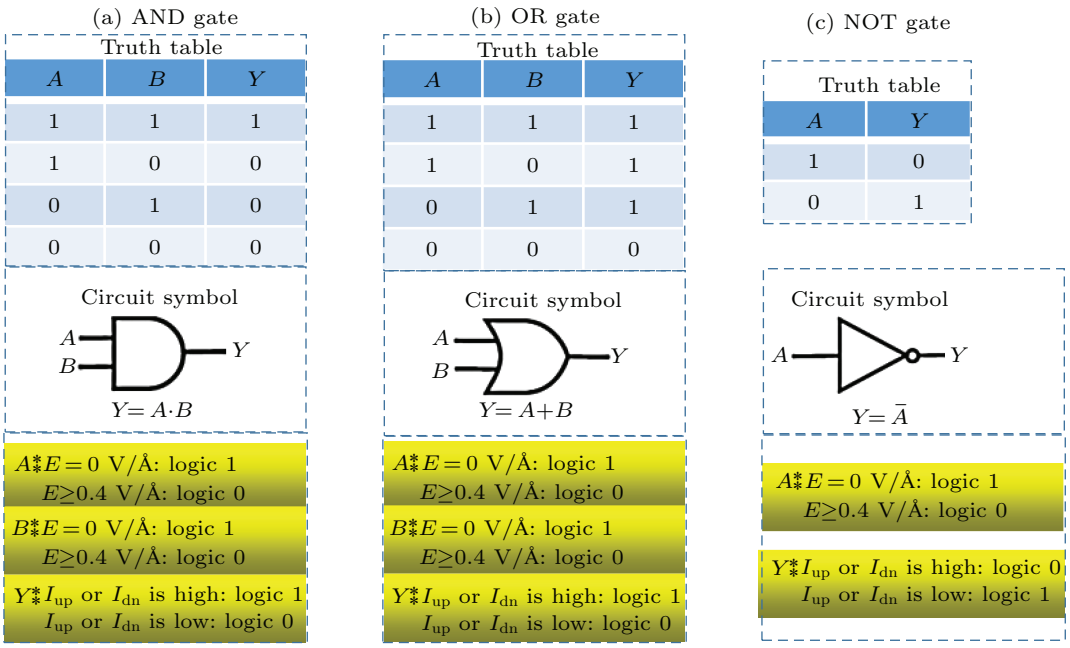


Fig. 8. The inputs, output, truth table, and circuit symbols for thermal spin MLGS, (a) AND, (b) OR, and (c) NOT.

4. Conclusion

In summary, the DFT + NEGF method was employed for the theoretical study of thermally-driven spin-related transport features of a single molecular device. The thermally-driven spin-related currents were successfully regulated by using the electric field based on the results. The thermally-driven spin-related transport features were employed to design three primary spin molecular gates (AND, OR, and NOT). The mentioned outcomes indicate the significant potential of the molecular devices for thermal spin molecular devices.

Acknowledgements

Project supported by the Natioanl Natural Science Foundation of China (Grant No. 11864011) and in part by Youth Project of Scientific and technological Research Program of Chongqing Education Commission (Grant No. KJQN202101204).

References

[1] Moore G E 1965 *Electronics* **38** 114
[2] Mathur N 2002 *Nature* **419** 573
[3] de Silva P, Gunaratne N and McCoy C 1993 *Nature* **364** 42
[4] Mikhail F B 2017 *Russ. Chem. Rev.* **86** 181
[5] Cai K, Yang M, Ju H, Wang S, Ji Y, Li B, Edmonds K W, Sheng Y, Zhang B and Zhang N 2017 *Nat. Mater.* **16** 712
[6] Yang M, Deng Y, Wu Z, Cai K, Edmonds K W, Li Y, Sheng Y, Wang S, Cui Y and Luo J 2019 *IEEE Electron Dev. Lett.* **40** 1554
[7] Zhang N, Cao Y, Li Y, Rushforth *A* W, Ji Y, Zheng H and Wang K 2020 *Adv. Electron. Mater.* **6** 2000296
[8] Cao Y, Rushforth A, Sheng Y, Zheng H and Wang K 2019 *Adv. Fun. Mater.* **29** 1808104
[9] Zhou J, Zhao T, Shu X, Liu L, Lin W, Chen S, Shi S, Yan X, Liu X and Chen J 2021 *Adv. Mater.* **33** 2103672
[10] Rinaldi G 2010 *Assembly Automation* **30** 2
[11] Sanvito S 2011 *Chem. Soc. Rev.* **40** 3336
[12] Wolf S, Awschalom D, Buhrman R, Daughton J, von Molnár V S, Roukes M, Chtchelkanova A Y and Treger D 2001 *Science* **294** 1488
[13] Uchida K, Takahashi S, Harii K, Ieda J, Koshibae W, Ando K, Maekawa S and Saitoh E 2008 *Nature* **455** 778
[14] Jaworski C M, Yang J, Mack S, Awschalom D D, Heremans J P and Myers R C 2010 *Nat. Mater.* **9** 898
[15] Uchida K, Xiao J, Adachi H, Ohe J, Takahashi S, Ieda J, Ota T, Kajiwara Y, Umezawa H, Kawai H, Bauer G E W, Maekawa S and Saitoh E 2010 *Nat. Mater.* **9** 894
[16] Zeng M, Feng Y and Liang G 2011 *Nano Lett.* **11** 1369
[17] Bauer G E W, Saitoh E and van Wees B J 2012 *Nat. Mater.* **11** 391
[18] Fu H, Wu D D, Zhang Z Q and Gu L 2015 *Sci. Rep.* **5** 10547
[19] Sierra J F, Neumann I, Cuppens J, Raes B, Costache M V and Valenzuela S O 2018 *Nat. Nanotechnol.* **13** 107
[20] Zhao P and Chen G 2019 *Chem. Phys. Lett.* **733** 136671
[21] Zhao P 2019 *J. Mag. Mag. Mater.* **489** 165381
[22] Zhao P and Chen G 2018 *J. Chem. Phys.* **149** 134305
[23] Zhang X Y and Zhao P 2020 *Phys. Lett. A* **384** 126256
[24] He H B and Zhao P 2020 *Physica E* **121** 114130
[25] Guo Y, Zhao P and Chen G 2022 *Chin. Phys. B* **31** 047202
[26] Brandbyge M, Mozos J L, Ordejon P, Taylor J and Stokbro K 2002 *Phys. Rev. B* **65** 165401
[27] Soler J M, Artacho E, Gale J D, García A, Junquera J, Ordejón P and Sánchez-Portal D 2002 *J. Phys.: Conden. Matt.* **14** 2745
[28] Perdew J P and Wang Y 1992 *Phys. Rev. B* **45** 13244
[29] Perdew J P, Burke K and Ernzerhof M 1996 *Phys. Rev. Lett.* **77** 3865
[30] Imry Y and Landauer R 1999 *Rev. Mod. Phys.* **71** S306
[31] Vergniory M, Granadino-Roldan J, Garcia-Lekue A and Wang L W 2010 *Appl. Phys. Lett.* **97** 262114
[32] Tobisu M and Chatani N 2014 *Science* **343** 850